

Universiteit
Leiden
The Netherlands

Probing quantum materials with novel scanning tunneling microscopy techniques

Bastiaans, K.M.

Citation
Bastiaans, K. M. (2019, December 10). *Probing quantum materials with novel scanning tunneling microscopy techniques*. *Casimir PhD Series*. Retrieved from https://hdl.handle.net/1887/81815

Version:	Publisher's Version
License:	Licence agreement concerning inclusion of doctoral thesis in the Institutional Repository of the University of Leiden
Downloaded from:	https://hdl.handle.net/1887/81815

Note: To cite this publication please use the final published version (if applicable).

Cover Page



Universiteit Leiden



The handle http://hdl.handle.net/1887/81815 holds various files of this Leiden University dissertation.

Author: Bastiaans, K.M.
Title: Probing quantum materials with novel scanning tunneling microscopy techniques
Issue Date: 2019-12-10

3

Charge trapping and super-Poissonian noise centers in a cuprate superconductor

This chapter has been published as *Nature Physics* **14**, 1183 (2018)

The electronic properties of cuprate high temperature superconductors in their normal state are highly two-dimensional: transport along the crystal planes is perfectly metallic, but is insulating along the perpendicular c-axis direction. The ratio of the in-plane and perpendicular resistance can exceed 10^4 (refs [1–4]). This anisotropy was identified as one of the mysteries of the cuprates early on [5, 6], and although widely different proposals exist for its microscopic origin [7–9], there is little empirical information on the microscopic scale. In this chapter, we elucidate the properties of the insulating layers with a newly developed scanning noise spectroscopy technique that can spatially map the current and its time-resolved fluctuations. We discover atomic-scale noise centres that exhibit MHz current fluctuations 40 times the expectation from Poissonian noise, more than what has been observed in mesoscopic systems [10]. Such behaviour can happen only in highly polarizable insulators and represents strong evidence for trapping of charge in the charge reservoir layers. Our measurements suggest a picture of metallic layers separated by polarizable insulators within a three-dimensional superconducting state.

3.1. INTRODUCTION

The difference between metals and insulators is that in the former, additional charge equilibrates in femtoseconds while the latter can be statically charged. The coupling to the lattice is a necessary condition for the trapping of charge in insulators on macroscopic timescales since electrons by themselves are too quantum mechanical to localize. The trapped charge is stabilized by the formation of static, localized polarons involving a reconfiguration of the atomic lattice. Strongly polarizable insulators such as SrTiO3 exemplify this process. Such trapping of charge on slow timescales has been conjectured as a cause of the anomalous, highly resistive c-axis transport in the cuprate high-temperature superconductors [7], competing with alternative proposals such as incoherent transport [11, 12]. We note that in these materials, bands structure theory predicts metallic transport along the c-axis due to the small but finite c-axis bandwidth of the order of 0.1 eV (ref. [13]). In this chapter, we present firm evidence that such charge trapping processes do occur in a superconducting cuprate material by measuring atomically resolved current fluctuations.

3.2. NOISE AS THE SIGNAL

Quite generally, fluctuations in time of a signal - the noise - can be a powerful diagnostic tool as they contain information not present in the mean value. It has historically allowed to distinguish between signals carried by particles and waves or between black body radiation and coherent radiation of a laser. More recently, noise spectroscopy has established itself as a standard method of investigating mesoscopic systems. This is usually done by looking at the noise spectral power, $S(w) =< \delta I(t)\delta I(t') >$, where δI is the deviation of the current operator from the mean, and the averaging <> is both quantum mechanical and statistical. Examples where noise transport measurements led to novel insight include: the study of fractional charge [14], the doubling of charge in Andreev processes (see chapter 4), and the vanishing of noise in break junctions at the quantum conductance [15]. We have succeeded in bringing this technique to the atomic scale in the tunnelling regime (see chapter 2), and in this chapter we show how we use this technique to discover an unanticipated phenomenon when we applied it to a cuprate high temperature superconductor.

The flow of classical, uncorrelated charged particles between two leads is a purely Poissonian process. Its noise is independent of frequency (white) and proportional to the charge q and the flow I of the carriers, $S = 2q|I|$, as a direct consequence of the discreteness of the carriers [16]. In chapter 2 we defined the normalized noise $S_n = S/2e|I|$, which shows the deviation from the Poissonian noise, similar to the Fano factor. Thus $S_n = 1$ represents Poissonian noise, $S_n < 1$ and $S_n > 1$ refer to sub-Poissonian and super-Poissonian noise, respectively (Fig. 3.1.a-b). For an uncorre-

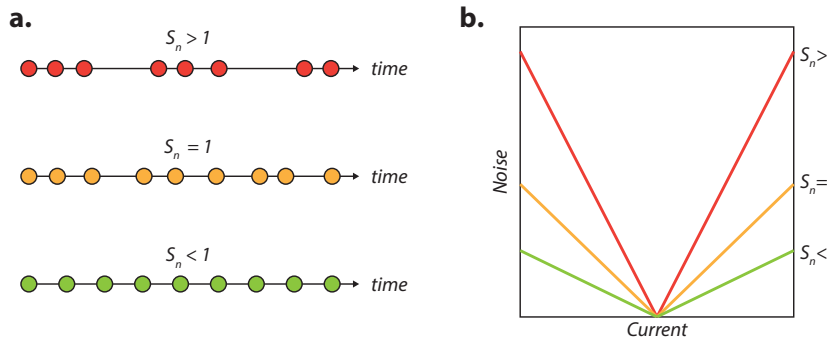


Figure 3.1: **Scanning tunnelling noise spectroscopy as a new diagnostic tool. a.** The classical flow of uncorrelated particles with charge q is a pure Poissonian process, $S = 2q|I|$. In the case of bunching, $S > 2q|I|$ and we refer to the noise as super-Poissonian (red). In the case of anti-bunching, $S < 2q|I|$ which is called sub-Poissonian (green). **b.** Noise S as a function of current in the cases described in (a).

lated electronic liquid, one expects $S_n = 1$; for an exotic, spatially inhomogeneous electronic liquid, this is a priori unclear. Importantly, in order to find $S_n > 1$, processes are required in the system on a frequency scale that fits into the slow (MHz) frequency window of the noise measurements. Another property of special relevance to our data is that such noise events may be completely invisible in the mean value of the current.

Our aim is thus to measure the fluctuations in the cuprates on the atomic scale. Bringing noise measurement to the tunnelling regime comes with unique challenges, as discussed in chapter 2, which prevented any atomic resolution shot noise measurement thus far. The central obstacle lies in the high impedance of the tunnelling junction, which is typically 0.3 GOhm to 10 GOhm. Together with the capacitance between tip and sample and the cable capacitance, the junction acts as low pass filter only allowing transmission of signals in the kHz range where $1/f$ noise and mechanical resonances dominate. Possible solutions include bootstrapping of an amplifier [17] or building an impedance matching circuit [18]. Matching a GOhm junction leads to considerable losses in the circuit. This is simplified when using the STM in point contact mode or in the low MOhm range [18, 19] or by using force-microscopy based methods [20], however, this increases interactions between tip and sample, making it more difficult to extrapolate the sample properties. Our goal is to perform noise measurements when in the tunnelling regime, with transparencies $\tau \sim 10^{-6}$. To accomplish this task, we build a new amplifier for scanning tunneling microscopy at MHz frequencies. The details of this amplification circuit that allows us to map out noise around 3 MHz with GOhm junction resistances are discussed in chapter 2.

3.3. DISCOVERY OF SUPER-POISSONIAN NOISE CENTERS

We choose to investigate cuprate high-temperature superconductors [21] first with this new scanning noise microscopy instrument, with the hope to find signs of the slow, glassy fluctuations associated with charge- and/or current loop order that have been claimed to show up in the noise [22–24]. We didn't observe any signs of these, but instead we found a surprise that we will explain in this chapter.

As a sample material, we decided to use the slightly overdoped bi-layer cuprate $(Pb,Bi)_2Sr_2CaCu_2O_{8+\delta}$ with $T_c = 79$ K. The Pb substitution for Bi has the advantage of supressing the characteristic supermodulation seen in many Bi based cuprates, simplifying the interpretation and making higher voltage measurements possible. We cleave the samples in UHV at pressures below 10^{-10} mbar, and directly insert them into our STM head at 3.2 K. The single crystal sample is held at a constant voltage V_{bias} which drops over the GOhm junction between the tip and the uppermost CuO layer. The tunnelling process starts with electrons originating from the CuO layer which then tunnel through the SrO and Bi layers [25]. Tunnelling through these charge reservoir layers does not have much effect on the STM signal, except for some spatial filtering [25, 26]. Figure 3.2.a shows a topographic image revealing atomic resolution. The square Bi-lattice is clearly resolved with some bright protrusions induced by Pb-substitutions for Bi atoms (see appendix 3.B).

Upon recording the noise as a function of spatial location with atomic resolution at bias voltages of ±0.1 eV we find homogeneously Poissonian noise, with no sign of the fluctuating orders. However, this changes dramatically when increasing the bias voltage, as shown in Figure 3.2.b-c. While most locations still exhibit Poissonian noise, a few atomic locations reveal striking enhancements of the noise. These super-Poissonian noise centers show noise values up to 40 times the expectation from Poissonian processes, more than anything that has been observed in mesoscopic systems [10]. We emphasise that the increase in noise is extremely localized, the width of the peaks in space being around 0.5 nm for most centers. The density of super-Poissonian noise centers is roughly 0.3% referenced to the number of Cu atoms, and they are evenly distributed throughout the sample.

3.4. NOISE SPECTROSCOPY ON NOISE CENTERS

A key insight comes from the energy dependence of the noise. Noise spectra are shown in Figure 3.2.d-f. Below a certain threshold, the noise in the tunnelling current is purely Poissonian, $S_n = 1$. But above around 1 eV or below around -650 meV the normalized noise rises rapidly. Surprisingly all noise centers appear to be highly asymmetric in energy: the noise enhancements at positive bias do not spatially correlate with the noise enhancement seen at negative energy. While different locations

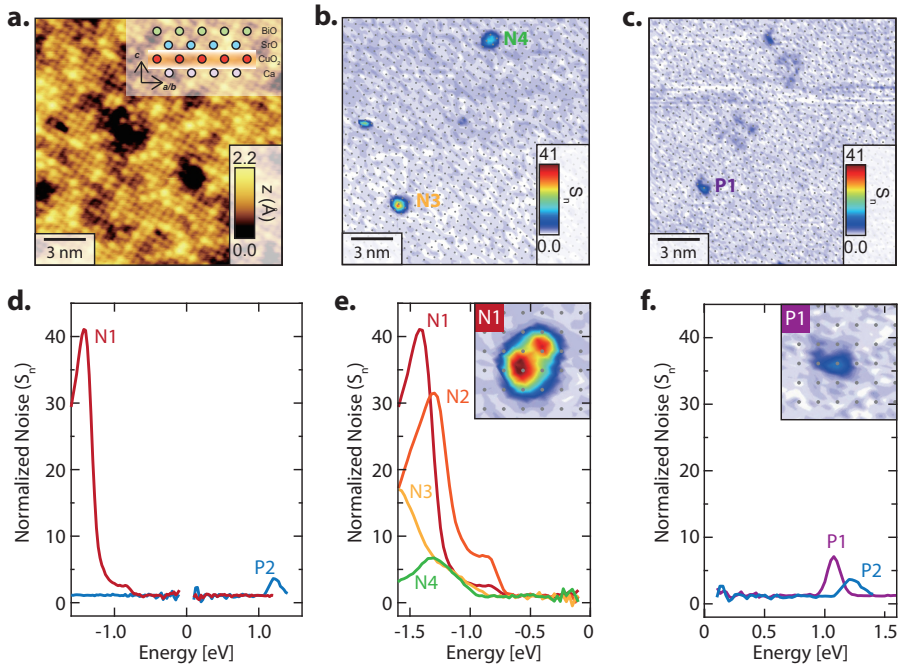


Figure 3.2: **Observation of super-Poissonian noise centers. a.** An atomic-resolution STM image of the BiO terminated overdoped bi-layer cuprate $(Pb,Bi)_2Sr_2CaCu_2O_{8+\delta}$ surface in a 18.3 nm field of view (sample bias $V_B = -0.10$V, current $I_S = 0.1$nA. Pb substitution for Bi are visible as bright protrusions. **b. c.** Spatially resolved, background line-subtracted, noise maps at -1.2 (b) and +1.1 (c) eV in the same field of view as figure 3.2a. The noise is normalized by the current simultaneously recorded at the same location. Most locations show homogeneous Poissonian noise ($S_n = 1$), but a few atomic locations reveal striking enhancements. N3, N4, and P1 indicate the negative and positive noise centers. Grey dots represent the Cu lattice sites. **d.** Representative noise spectra on the atomic locations that exhibit super-Poissonian noise show the strong asymmetry. **e. f.** Noise spectra on various positive and negative noise centers. Each inset shows the spatial distribution of the noise enhancements.

show different strengths of noise enhancement, the onset energy seems to be independent of the noise center, roughly -0.8 eV for the negative energy noise centers, and roughly +1 eV for the positive ones. This indicates a common mechanism and turns out to be an important diagnostic tool, as discussed below.

To understand these observations, it is worth taking a step back and look at engineered and natural systems that exhibit non-Poissonian noise, $S_n \neq 1$. In electronic systems this is most often sub-Poissonian noise [10, 12, 15, 17], usually due to sequential tunneling in quantum dots or Pauli exclusion effects. However, in the tunneling regime considered here ($\tau \sim 10^{-6}$), the latter are minimal. Super-Poissonian noise on the other hand is a much rarer occurrence, as it always has to include some sort of interaction [10]. Experimentally, super-Poissonian noise was first observed in semiconductor double-wells and later in quantum dots [27]. Examples of super-

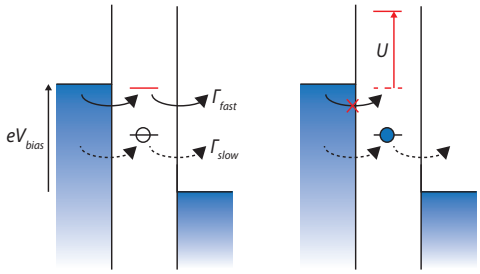


Figure 3.3: **Example of modulated transport by slow charge trapping processes.** Energy diagram of the co-tunnelling process via impurity states. Two tunnelling processes are possible; one of them has higher transmission rate than the other and dominates the total tunnelling current. Since they are strongly coupled by Coulomb energy (U), the tunnelling through the higher impurity level is prohibited by charge trapping of the lower one.

Poissonian noise include bi-stable systems that lead to random telegraph noise in the transport, and coupling to inelastic modes [28]. Our data allows us to exclude all these mechanisms as the observed noise is bias dependent and asymmetric.

3.5. MODULATED TRANSPORT BY POLARONIC CHARGE TRAPPING

Instead, our data suggests the following scenario known from double quantum dots, as illustrated in Fig. 3.3. Two tunneling processes are present, one fast, accounting for almost all the tunneling current, and one slow, acting as a switch for the first one. This switching mechanism is usually based on Coulomb interaction. For example, if the state of the slow process is occupied, it raises the energy level of the state necessary for the fast process and effectively blocks it, as shown in Fig. 3.3. This leads to an effective switching i.e. bunching of electrons that causes super-Poissonian noise. Such mechanisms have been discussed in detail for mesoscopic systems [10, 12, 29] and confirmed by experiments in double quantum dots [30]. We note that this scenario (i) predicts a clear threshold energy after which the noise increases, (ii) is asymmetric with respect to energy, (iii) is localized on the atomic scale. The key insight that follows from our observations is that some slow process is involved, i.e. a form of charge trapping that is known from strongly polarizable insulators but not from a metal.

One expects these noise centers to correspond with some form of polarons being localized at defects in the crystal lattice, in contrast to more itinerant polarons at other locations. To shed light on their precise nature, we searched for impurity states, following earlier work [31] but now taking fully normalized dI/dV / (I/V) density of states maps over a large energy range to be able to differentiate impurity states that

overlap in energy. The energy dependent dI/dV / (I/V) maps reveal the spatial distribution of the different impurity states. Such states have been identified as (i) apical oxygen vacancies, (ii) Sr(Ca)-site impurities, (iii) interstitial oxygen dopants and (iv) Pb impurities. Figure 3.4 shows signatures of these specific states; details can be found in appendix 3.B.

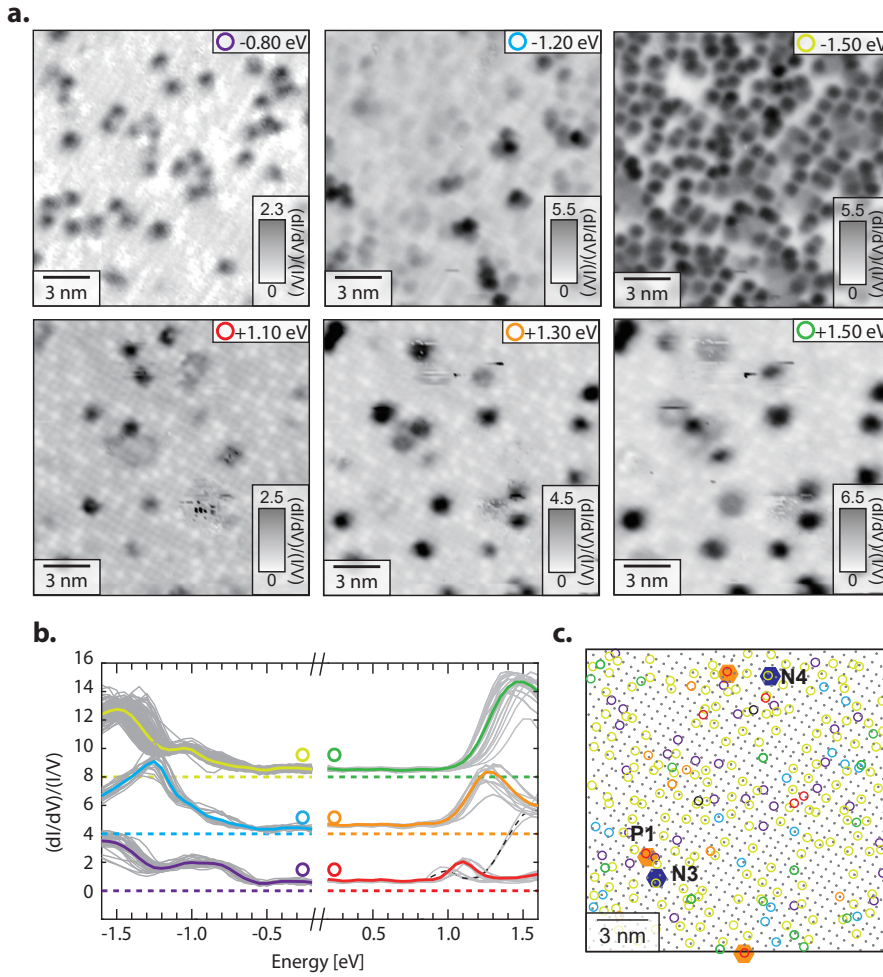


Figure 3.4: **Bias-dependent conductance maps to identify impurity states and correlation with noise centers. a.** Density of states at different energy levels: -1.5, -1.2, -0.8, +1.1, +1.3, and +1.5 eV. They were acquired in the same field of view as in Fig. 3.2a. The enhancement in normalized differential conductance ((dI/dV)/(I/V)) reveals the spatial distribution of various impurity states. **b.** Normalized differential conductance spectra taken on the different impurity states in Fig. 3.4a. The thick colored lines represent the average of the individual grey spectra. **c.** Overview of all impurity states in this field of view. Grey dots display the Cu-lattice. Various symbols corresponding to the different impurity states classified based on (a). The noise centers are indicated by the blue (negative) and red (positive) hexagons.

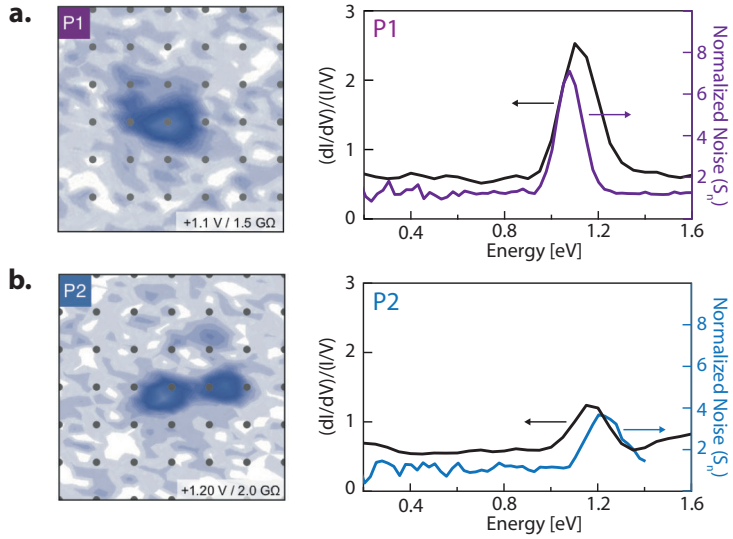


Figure 3.5: **Correspondence between the positive energy noise centers and the +1.1V impurity state. a.** Positive noise center P1 from Fig. 3.2. **b.** Positive noise center P2 from Fig. 3.2.

Most importantly, we find a clear correspondence between positive-energy noise centers and the +1.1 V impurity state, as shown in Fig. 3.4.c and 3.5. This impurity state has previously been identified as an apical oxygen vacancy [31] which, in the insulating oxygen materials, has various charge states stabilized by lattice distortions. This amounts to strong evidence for this signature to be associated with the charge trapping process. The positive noise centers show all this signature of an impurity state in the charge reservoir layer through which tunneling occurs but modulated by a slow charge trapping process. Surprisingly, we do not observe a clear correspondence between a specific type of impurity resonance and the site of the negative noise centers. This might be because the state is dark due to filtering mechanisms [26], or because of stronger coupling to the CuO layer.

3.6. CONCLUSIONS AND OUTLOOK

In this chapter we have presented direct evidence for the existence of slow charge trapping processes at defect sites in the form of the localized super-Poissonian noise signals. These are reminiscent of Coulombic impurities that occur generically in polarizable insulators, despite the three-dimensional superconducting state present in our samples. While the atomic centers with noise enhancement are sparse, they demonstrate the polaronic nature of charge carriers tunneling through the insulating layers. Apart from the noise centers, the polarons are likely itinerant to different

degrees; a situation that at present cannot be described by theory. The c-axis physics of the cuprates thus appears to be in a quite literal sense similar as to what is found in e.g. the aluminum oxide barriers employed for Josephson junctions: No coherent charge transport is possible for normal electrons, while the virtual tunnelling of Cooper pairs suffices for a coherent Josephson contact. In the cuprates, this is manifested of the form of the c-axis Josephson plasmons observed in the optical conductivity [32], emerging from a completely overdamped charge transport in the normal state [3]. The surprise is that apparently an oxidic layer that is only two atoms thick living in a metallic environment suffices for the polaronic trapping of charge.

The role of the 'c-axis phenomena' in the mechanism of high-temperature superconductivity is a long standing question [5, 6, 32], as is the unusual nature of the coupling of the polar insulator phonons to the electrons [5, 6, 8, 9, 33]. This acquired new impetus recently with the discovery that when a single layer of FeSe is removed from bulk and put on an polarizable insulator, the critical temperature increases by a factor of four [34], with evidence reported suggesting that the coupling to the polarizable insulating substrate may indeed play a critical role [35]. Further, interfaces of the polarizable insulators $SrTiO_3$ and $LaAlO_3$ host two dimensional superconductors with the highest T_c per charge density ratio [33]. So much is clear from our findings that even for the atomically thin insulating layers the polar electron-phonon interactions are of a severity sufficing to slow down electronic motions to macroscopic time scales. Although a great challenge for established theory, this conundrum deserves further close consideration.

APPENDICES

3.A. CORRELATION TO LOW-ENERGY FEATURES

We also correlated the atomic locations of the observed noise enhancement sites to the low-energy features known in Bi-based cuprate samples. Spectroscopic imaging STM has proven to be a very powerful tool for visualizing these low-energy features. By recording the dI/dV (proportional to the LDOS) spectrum over a spatially distributed grid of point we construct a three-dimensional dataset of the electronic structure as function of energy and the spatial coordinates. From this dataset we can then abstract the low-energy features like the superconducting gap magnitude (Fig. 3.6.b) or charge order arrangements in the electronic structure (Fig. 3.6.c). By recording an atomically resolved noise map (Fig. 3.6.a) in the same field of view at high energy we can correlate these low energy features of the sample to the noise enhancement centers we identified in this chapter. Visual comparison does not reveal any correlation between the noise enhancement sites and the low energy features (Fig. 3.6).

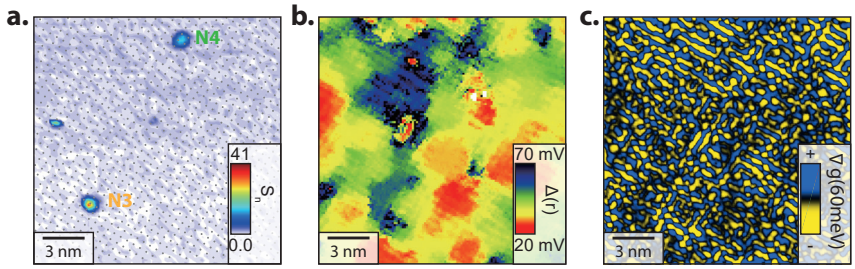


Figure 3.6: **Correlation of observed noise centers with low energy features. a.** Spatially resolved noise map at -1.2eV at a 20 nm field of view. The negative noise centers exhibit enhancements of 10 times Poissonian noise and are indicated by the white circles. **b.** Spatial map of the superconducting gap magnitude over the sample surface in the same field of view as (a). The white circles indicate the locations of the negative noise centers. **c.** Laplacian of the ratio of the conduction maps at 52 meV and -52 meV in the same field of view, for better visualization of the atomic-scale arrangements of the spatial pattern.

3.B. DETERMINATION OF IMPURITY STATES

It is well known that there are several impurity states at high binding energy in $(Pb,Bi)_2Sr_2CaCu_2O_{8+\delta}$ samples [36]. Based on previous reports we expect that there are five kinds of impurities states, originating from type-A, type-B, apical oxygen vacancies [31], Pb^{2+} substitutions for Bi^{3+}, and Bi^{3+} substitutions for Sr^{2+} [37]. They are located at a binding energy of -1.5, -1.0, +1.0, -1.4, and +1.7 eV, respectively. Since all of the noise enhancement centers are observed at the high binding

energy regime, we want to identify all of impurity states in $(Pb,Bi)_2Sr_2CaCu_2O_{8+\delta}$ and check the correlation with the noise enhancement sites.

The conductance maps shown in Fig. 3.7 were acquired for the same field of view of noise maps shown in Fig. 3.2 using the typical spectroscopy technique. The setup conditions for the positive and negative bias maps are +1.60 and -1.60 V / 0.10 nA respectively. We used a lock-in modulation of 50 mV at 887 Hz. The STM images taken at the high bias have strong corrugations induced by the impurity states and thus the so called set-up effect is not negligible. To minimize these artifacts, we used the normalized local density of states by dividing dI/dV by I/V, which is a better measure of LDOS modulations in the present case. We thoroughly checked LDOS maps of all energy levels to identify all kinds of impurity states. There are six energy levels, -1.50, -1.20, -0.80, +1.10, +1.30, and +1.50 eV, which exhibit different impurity distributions. In Fig. 3.7.a, the colored circles on negative energy LDOS maps highlight local maxima. By overlaying the impurity maps for the filled states, we reveal that three separate impurities rarely coexist at the same site. Also all dI/dV spectra taken at these local maxima in Fig. 3.4.b show similar behavior. Therefor both the averaged spectra and the LDOS maps are usable for identifing the spectral feature of the impurity and their spatial distributions. From our analysis of the LDOS layers, we reveal that the LDOS map at -1.50 eV and the average spectra acquired at the local maxima are identical to the Pb impurity state. By comparison with previous studies, the impurity states around -1.20 and -0.80 eV are related with interstitial oxygen impurities. Previous theoretical study expected that one of interstitial oxygen impurities located close to SrO layer show a clear anti-correlation with inhomogeneous pseudogap due to hole-doping on CuO_2 layer [38]. It was also experimentally shown in a high doped sample on the atomic scale [31]. However, we note that in our measurements the -1.2 eV state does not show a clear anti-correlation with the pseudogap, but a stronger correlation than the -0.8 eV impurity states. The latter are randomly distributed, the former tend to be located in the smaller pseudogap region. Therefore, we identify the -1.2 and -0.8 eV impurity states as the interstitial oxygen impurities around SrO and BiO layer, respectively.

To classify the impurity states at positive bias, we need one more procedure since different impurities exhibit similar contrast in the LDOS map at certain energies. The impurity map (Fig. 3.7.b) clearly shows several colored circles marked at the same atomic site. We sort collected spectra taken at the position according to the peak positions. According to our classifications shown in Fig. 3.4.b, there are at least 3 types of impurities which have a resonance peak above +0.9 eV. So far, only two impurities, apical oxygen vacancy and Bi^{3+} substitutions for Sr^{2+}, have been reported to have impurity states at the positive bias. The previous STS results [31] reported that the apical oxygen vacancies have the impurity state around +1.0 eV and exhibits a clear correlation with the pseudogap due to the local reduction of the hole concentration.

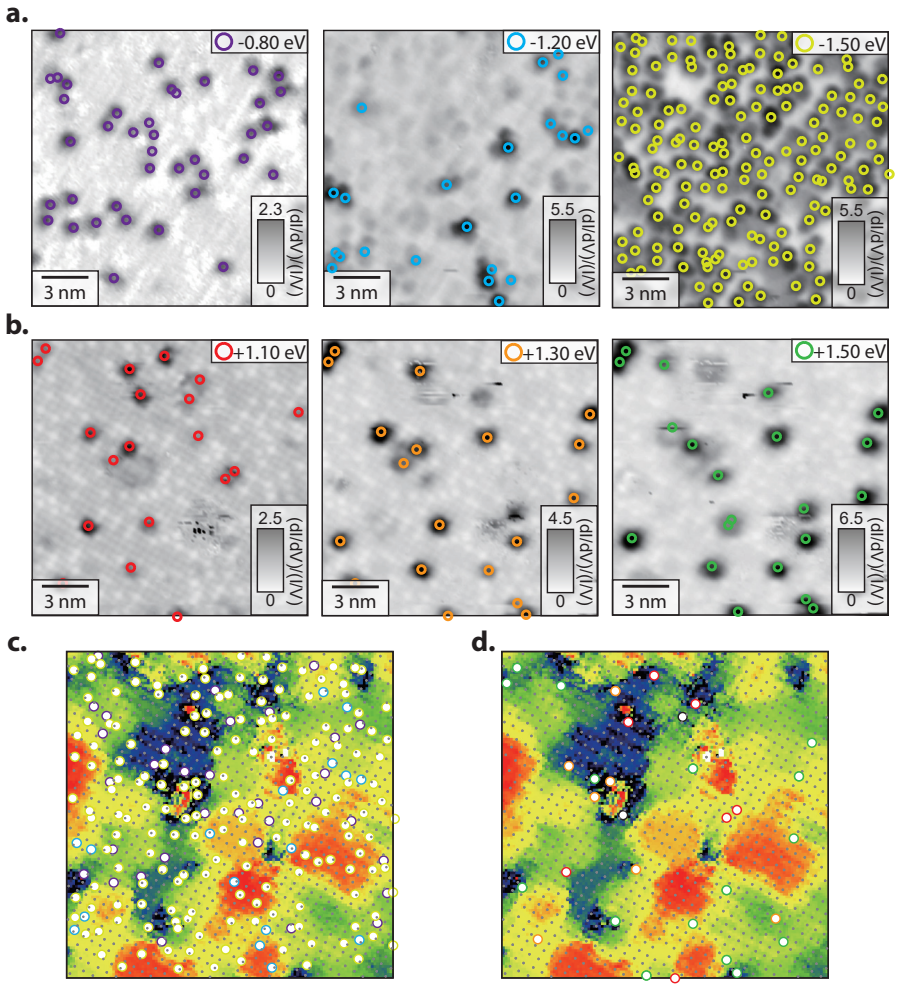


Figure 3.7: **Identification of impurity states. a and b.** The energy dependent normalized density of states maps dI/dV/(I/V) maps for high negative and positive bias. The colored circles highlight the local maxima of the maps and correspond to the locations of impurities. The schematics are made by superimposing all of impurity markers. The dashed circles indicate the sites where the impurities coexist. **c and d.** Comparison between impurity site and inhomogeneous pseudogap. The impurity maps (same with Fig. 3.4) for negative (c) and positive (d) impurity state are superimposed on the pseudogap map.

This is consistent with one of our impurities whose spectra have a peak at 1.1 eV. The other two impurity states have similar atomic-scale feature (Fig. 3.4.a) and spectral shape (Fig. 3.4.b). We therefore identify these impurities as donor levels originated from Bi^{3+} substitutions for Sr^{2+}.

3.C. VARIOUS SUPER-POISSONIAN NOISE CENTERS

In this Fig. 3.8 we display the spatially resolved noise maps of the noise centers mentioned in Fig. 3.2.

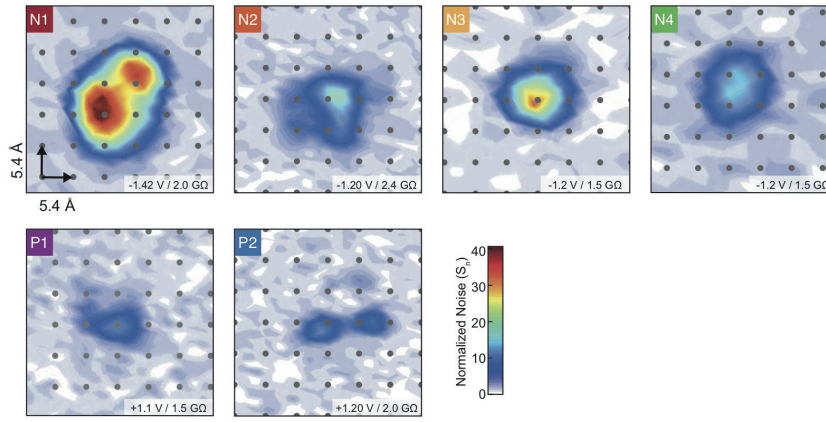


Figure 3.8: **Various super-Poissonian noise centers**, as referred to in Fig. 3.2. The grey dots display the Cu-lattice.

BIBLIOGRAPHY

[1] T. Watanabe, T. Fujii, and A. Matsuda, *Anisotropic resistivities of precisely oxygen controlled single-crystal bi 2 sr 2 cacu 2 o 8+ δ: Systematic study on"spin gap"effect,* Phys. Rev. Lett. **79**, 2113 (1997).

[2] G. Sordi, P. Semon, K. Haule, and A.-M. Tremblay, *c-axis resistivity, pseudogap, superconductivity, and widom line in doped mott insulators,* Phys. Rev. B **87**, 041101 (2013).

[3] J. Levallois, M. Tran, D. Pouliot, C. Presura, L. Greene, J. Eckstein, J. Uccelli, E. Giannini, G. Gu, A. Leggett, and D. van der Marel, *Temperature-dependent ellipsometry measurements of partial coulomb energy in superconducting cuprates,* Phys. Rev. X **6**, 031027 (2016).

[4] J. H. Kim, H. Somal, M. Czyzyk, D. Van der Marel, A. Wittlin, A. Gerrits, V. Duijn, N. Hien, and A. Menovsky, *Strong damping of the c-axis plasmon in high-tc cuprate superconductors,* Physica C: Superconductivity **247**, 297 (1995).

[5] P. Anderson, *Experimental constraints on the theory of high-tc superconductivity,* Science **256**, 1526 (1992).

[6] A. Leggett, *A "midinfrared" scenario for cuprate superconductivity,* PNAS **96**, 8365 (1999).

[7] D. Gutman and D. Maslov, *Anomalous c-axis transport in layered metals,* Phys. Rev. Lett. **99**, 196602 (2007).

[8] S. Johnston, F. Vernay, B. Moritz, Z.-X. Shen, N. Nagaosa, J. Zaanen, and T. Devereaux, *Systematic study of electron-phonon coupling to oxygen modes across the cuprates,* Phys. Rev. B **82**, 064513 (2010).

[9] W. Meevasana, T. Devereaux, N. Nagaosa, Z.-X. Shen, and J. Zaanen, *Calculation of overdamped c-axis charge dynamics and the coupling to polar phonons in cuprate superconductors,* Phys. Rev. B **74**, 174524 (2006).

[10] Y. Blanter, *Recent advances in studies of current noise.* in *CFN Lectures on Functional Nanostructures-Volume 2* (Springer, Berlin, Heidelberg, 2011).

[11] P. W. Anderson and Z. Zou, *"normal" tunneling and "normal" transport: Diagnostics for the resonating-valence-bond state,* Phys. Rev. Lett. **60**, 132 (1988).

[12] P. Moses and R. H. McKenzie, *Comparison of coherent and weakly incoherent transport models for the interlayer magnetoresistance of layered fermi liquids,* Phys. Rev. B **60**, 7998 (1999).

[13] R. S. Markiewicz, S. Sahrakorpi, M. Lindroos, H. Lin, and A. Bansil, *One-band tight-binding model parametrization of the high-T_c cuprates including the effect of k_z dispersion,* Phys. Rev. B **72**, 054519 (2005).

[14] R. De-Picciotto, M. Reznikov, M. Heiblum, V. Umansky, G. Bunin, and D. Mahalu, *Direct observation of a fractional charge,* Nature **389**, 162 (1997).

[15] H. Van den Brom and J. Van Ruitenbeek, *Quantum suppression of shot noise in atom-size metallic contacts,* Phys. Rev. Lett. **82**, 1526 (1999).

[16] Y. M. Blanter and M. Büttiker, *Shot noise in mesoscopic conductors,* Physics Reports **336**, 1 (2000).

[17] H. Birk, M. De Jong, and C. Schönenberger, *Shot-noise suppression in the single-electron tunneling regime,* Phys. Rev. Lett. **75**, 1610 (1995).

[18] U. Kemiktarak, T. Ndukum, K. Schwab, and K. Ekinci, *Radio-frequency scanning tunnelling microscopy,* Nature **450**, 85 (2007).

[19] A. Burtzlaff, A. Weismann, M. Brandbyge, and R. Berndt, *Shot noise as a probe of spin-polarized transport through single atoms,* Phys. Rev. Lett. **114**, 016602 (2015).

[20] M. G. Sung, H. Lee, K. Heo, K.-E. Byun, T. Kim, D. H. Seo, S. Seo, and S. Hong, *Scanning noise microscopy on graphene devices,* ACS Nano **5**, 8620 (2011).

[21] B. Keimer, S. A. Kivelson, M. R. Norman, S. Uchida, and J. Zaanen, *From quantum matter to high-temperature superconductivity in copper oxides.* Nature **518**, 179 (2015).

[22] E. W. Carlson, K. A. Dahmen, E. Fradkin, and S. A. Kivelson, *Hysteresis and noise from electronic nematicity in high-temperature superconductors,* Phys. Rev. Lett. **96**, 097003 (2006).

[23] S. A. Kivelson, I. P. Bindloss, E. Fradkin, V. Oganesyan, J. M. Tranquada, A. Kapitulnik, and C. Howald, *How to detect fluctuating stripes in the high-temperature superconductors,* Rev. Mod. Phys. **75**, 1201 (2003).

[24] J. Zhang, Z. Ding, C. Tan, K. Huang, O. O. Bernal, P.-C. Ho, G. D. Morris, A. D. Hillier, P. K. Biswas, S. P. Cottrell, H. Xiang, X. Yao, D. E. MacLaughlin, and L. Shu, *Discovery of slow magnetic fluctuations and critical slowing down in the pseudogap phase of yba2cu3oy,* Science Advances **4** (2018).

[25] P. Choubey, A. Kreisel, T. Berlijn, B. M. Andersen, and P. J. Hirschfeld, *Universality of scanning tunneling microscopy in cuprate superconductors,* Phys. Rev. B **96**, 174523 (2017).

[26] I. Martin, A. V. Balatsky, and J. Zaanen, *Impurity states and interlayer tunneling in high temperature superconductors,* Phys. Rev. Lett. **88**, 097003 (2002).

[27] E. Onac, F. Balestro, B. Trauzettel, C. Lodewijk, and L. Kouwenhoven, *Shot-noise detection in a carbon nanotube quantum dot,* Phys. Rev. Lett. **96**, 026803 (2006).

[28] A. Thielmann, M. H. Hettler, J. König, and G. Schön, *Cotunneling current and shot noise in quantum dots,* Phys. Rev. Lett. **95**, 146806 (2005).

[29] S. S. Safonov, A. K. Savchenko, D. A. Bagrets, O. N. Jouravlev, Y. V. Nazarov, E. H. Linfield, and D. A. Ritchie, *Enhanced shot noise in resonant tunneling via interacting localized states,* Phys. Rev. Lett. **91**, 136801 (2003).

[30] S. Gustavsson, R. Leturcq, B. Simovič, R. Schleser, P. Studerus, T. Ihn, K. Ensslin, D. C. Driscoll, and A. C. Gossard, *Counting statistics and super-poissonian noise in a quantum dot: Time-resolved measurements of electron transport,* Phys. Rev. B **74**, 195305 (2006).

[31] I. Zeljkovic, Z. Xu, J. Wen, G. Gu, R. S. Markiewicz, and J. E. Hoffman, *Imaging the impact of single oxygen atoms on superconducting bi2+ysr2–ycacu2o8+x,* Science **337**, 320 (2012).

[32] A. Tsvetkov, D. Van der Marel, K. Moler, J. Kirtley, J. De Boer, A. Meetsma, Z. Ren, N. Koleshnikov, D. Dulic, A. Damascelli, M. Gruninger, J. Schutzman, J. Van der Eb, H. Somal, and J. Wang, *Global and local measures of the intrinsic josephson coupling in tl 2 ba 2 cuo 6 as a test of the interlayer tunnelling model,* Nature **395**, 360 (1998).

[33] N. Reyren, S. Thiel, A. D. Caviglia, L. F. Kourkoutis, G. Hammerl, C. Richter, C. W. Schneider, T. Kopp, A.-S. Rüetschi, D. Jaccard, M. Gabay, D. A. Muller, J.-M. Triscone, and J. Mannhart, *Superconducting Interfaces Between Insulating Oxides,* Science **317**, 1196 (2007).

[34] Q.-Y. Wang, Z. Li, W.-H. Zhang, Z.-C. Zhang, J.-S. Zhang, W. Li, H. Ding, Y.-B. Ou, P. Deng, K. Chang, J. Wen, C.-L. Song, K. He, J.-F. Jia, S.-H. Ji, Y.-Y. Wang, L.-L. Wang, X. Chen, X.-C. Ma, and Q.-K. Xue, *Interface-Induced High-Temperature Superconductivity in Single Unit-Cell FeSe Films on SrTiO3,* Chinese Physics Letters **29**, 037402 (2012).

[35] J. Lee, F. Schmitt, R. Moore, S. Johnston, Y.-T. Cui, W. Li, M. Yi, Z. Liu, M. Hashimoto, Y. Zhang, D. Lu, T. Devereaux, D.-H. Lee, and Z.-X. Shen, *Interfacial mode coupling as the origin of the enhancement of t c in fese films on srtio 3,* Nature **515**, 245 (2014).

[36] I. Zeljkovic and J. E. Hoffman, *Interplay of chemical disorder and electronic inhomogeneity in unconventional superconductors,* Physical Chemistry Chemical Physics **15**, 13462 (2013).

[37] G. Kinoda, H. Mashima, K. Shimizu, J. Shimoyama, K. Kishio, and T. Hasegawa, *Direct determination of localized impurity levels located in the blocking layers of* $bi_2sr_2Cacu_2o_y$ *using scanning tunneling microscopy/spectroscopy,* Phys. Rev. B **71**, 020502 (2005).

[38] S. Zhou, H. Ding, and Z. Wang, *Correlating off-stoichiometric doping and nanoscale electronic inhomogeneity in the high-T_c superconductor* $bi_2sr_2cacu_2o_{8+\delta}$, Phys. Rev. Lett. **98**, 076401 (2007).